Lawrence Berkeley National Laboratory
Recent Work

Title
SASSY, A GAS FILLED MAGNETIC SEPARATOR FOR THE STUDY OF FUSION REACTION PRODUCTS

Permalink
https://escholarship.org/uc/item/1mk1b1dm

Author
Ghiorso, A.

Publication Date
1987-11-01

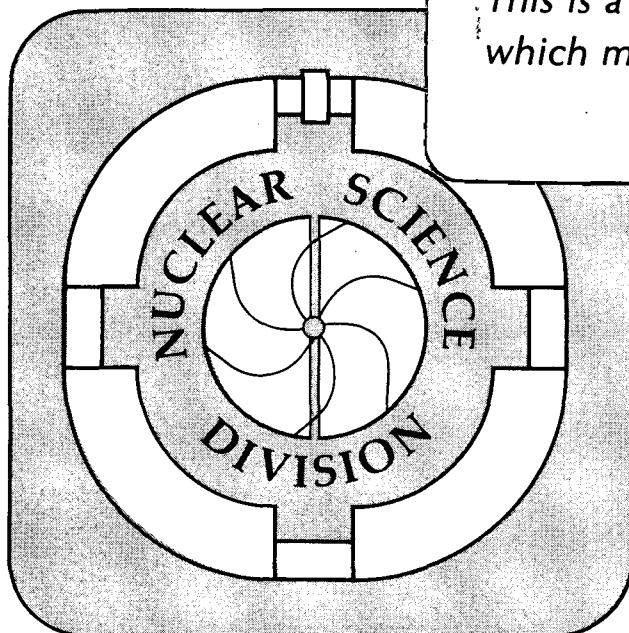# Lawrence Berkeley Laboratory

UNIVERSITY OF CALIFORNIA

SASSY, A Gas Filled Magnetic Separator for the Study of Fusion Reaction Products

A. Ghiorso, S. Yashita, M.E. Leino,
L. Frank, J. Kalnins, P. Armbruster,
J.-P. Dufour, and P.K. Lemmertz

November 1987

LBL-21975 c.2

DISCLAIMER

SASSY, A Gas Filled Magnetic Separator for the Study of Fusion Reaction Products

A. Ghiorso, S. Yashita, M.E. Leino,* L. Frank, J. Kalnins
Lawrence Berkeley Laboratory
University of California,
Berkeley, CA 94720

P. Armbruster, J.-P. Dufour,** P.K. Lemmertz
Gesellschaft für Schwerionenforschung, GSI
D-6100 Darmstadt
Fed. Rep. of Germany

Abstract

A gas-filled on-line recoil separator at the Berkeley SuperHILAC is described. The separator consists of a magnetic dipole and a quadrupole doublet. The system is filled with He at a pressure of about 1 Torr ($\sim$130 Pa). It separates particles according to their average magnetic rigidity. This allows a separation of evaporation residues, scattered target atoms and beam projectiles in a nuclear reaction.

The separation time is in the order of 10^{-6} s; the transmission is about 50% for evaporation residues, less than 10^{-3} for scattered target-like recoil ions and transfer products, and about 10^{-15} for full energy beam projectiles. Experimental data over a wide range of reactions are given and it is shown that the average charge of the recoils is determined by the atomic shell structure of the moving ionized atom in the gas.

1. Introduction

SASSY is an acronym for Small Angle Separating System. This instrument is designed to separate the evaporation residues of fusion reactions from intense projectile beams of heavy ions from the SuperHILAC. The separation of particles with a large spread in energy and charge can

be achieved either by a combination of electric and magnetic fields as is done in SHIP[1] or by a single magnetic dipole field if the field region is filled with a gas at low pressure. In the latter case collisions with the gas atoms continuously change the charges of the recoil particles along their paths so that the trajectory of each particle is determined by its average charge $\bar{q}$. This average charge is found to be independent of the initial charge distribution and roughly proportional to the velocity of the particles. This mechanism results in charge and velocity focusing and the gas-filled separator acts as a mass separator. This separation method was first developed by Cohen and Fulmer[2] in 1958 for fission products. A few years later the technique was used in a more sophisticated fashion by Armbruster et al.,[3,4] again for the separation of individual fission products. Independently, the principle was conceived and tested by Ghiorso in 1959 using the large steering magnet at the exit end of the HILAC to separate fusion recoils from a heavy ion beam. The simple experiment was set up for only a short time to test the idea. Although the test was encouraging, further development was not pursued for a number of years because of the press of other projects. At Dubna a gas-filled separator was used by Karnaukhov et al.[5] for the on-line identification of neutron-light Rare Earth evaporation residues produced in heavy ion reactions.

In 1971 Armbruster et al.[6] discussed the question of the more general separation capabilities of the gas-filled method to evaporation residues, transfer products and beam projectiles. In the present paper we will present some experimental answers to that question. Recently two papers have been published describing experiments performed in the Po and At regions with SASSY by Leino et al. and Yashita.[7] More recently further technical development of this device was undertaken to enhance its use for the superheavy reaction ^{48}Ca + ^{248}Cm. This lead to the necessity of extrapolating the calibration to high nuclear charge in combination with a low recoil velocity and prompted a systematic study of average equilibrium charges in He gas for a wide variety of evaporation residues. This paper mainly addresses itself to this interesting problem in atomic physics.

2. Principle of Operation

Let us consider a gas-filled magnetic dipole with a magnetic flux density B. An ion with mass A, charge q and velocity v will then move on a trajectory of radius ρ. In our case, B and v are perpendicular and the magnetic rigidity is given in tesla meters by Eq. 1.

$$B\rho = 0.0227 \, A \, \frac{\frac{v}{v_o}}{q} \, ,$$ (1)

where the velocity is expressed in units of the Bohr velocity $v_o = 2.19 \times 10^6$ m/s.

Strictly speaking, Eq. 1 describes a piecewise continuous trajectory with well defined q for each piece, as q fluctuates around a mean value $\bar{q}$ due to the charge exchange processes in collisions of the ion and the gas. For normal operating conditions the number of collisions is large and the energy loss is small. Experiments show that the trajectories can therefore be described by the initial velocity and the average charge $\bar{q}$.

The average ionic charge $\bar{q}$ of an atom depends on its atomic number Z and its velocity, and on the atomic number and density of the gas in which it moves. It is obvious that any experiment with a gas-filled separator requires a knowledge of $\bar{q}$ as a function of these parameters. Aside from gas-filled separators, the design of certain heavy ion accelerators and high resolution ionization chambers and the understanding of the energy loss mechanism must also deal with this complex problem. The most recent review of this field is by Betz.[8]

We will first use the theory of Bohr[9] to outline the main features of a gas-filled separator. For numerical calculations we have to rely on semiempirical formulas or on a model proposed by Lamb.[10] Bohr has predicted that all electrons with orbital velocities smaller than v are stripped. From the Thomas-Fermi model of the atom their number is calculated to be

$$\bar{q} = \left(\frac{v}{v_o}\right) Z^{1/3} \, ,$$ (2)

for a velocity range $1 < v/v_o < Z^{2/3}$.

Then Eq. 1 can be rewritten as

$$B\rho = 0.0227 \frac{A}{Z^{1/3}} \quad \text{in tesla meters .} \tag{3}$$

Equation 3 shows the two important first order properties of the gas-filled separator: $B\rho$ is independent of the velocity and of the initial charge distribution of the particles. It also allows a rough estimation of the separation properties of a gas-filled separator. For a symmetric target-projectile combination, we calculate a ratio of rigidities of 1:0.6:0.6 for evaporation residues, scattered target atoms and beam particles.

For a very asymmetric system like ^{48}Ca + ^{248}Cm we expect ratios of 1:0.9:0.3, i.e., the high intensity beam will be well separated and the evaporation residues and the scattered target atoms will still be separated by 10%. The focal plane of SASSY covers a maximum dispersion of $\sim$20% in $\frac{\Delta B\rho}{B\rho}$. EVR's and target knock-ons will be detected simultaneously at the same time that the primary beam is being strongly suppressed.

3. Description of the Separator

The main components of SASSY are shown schematically in Fig. 1. They are a 13" × 36" C-magnet with a 3" vertical aperture, followed immediately by two 8" dia. × 16" long quadrupole magnets, the first horizontally and the second vertically focusing. The dipole magnet has a central radius of curvature of 2.18 meters and a deflection angle of 23°. The separated beam of evaporation residues emerges from the dipole and it is then focused by the quadrupole doublet to the detector box. The total path length is 4 meters and it is filled with helium gas at a pressure of about 100 Pa.

The angular acceptance of the instrument without collimation is ±74 mrad horizontally and ±25 mrad vertically. At the focal plane in the detector box the optical magnification is 3.3 in the horizontal and 0.44 in the vertical direction. The dispersion in magnetic rigidity is 6.7 mm per % difference in $B\rho$.

The beam window (from 30 to 250 $\mu g/cm^2$ Al) with a diameter of 6 mm is located at the upstream edge of the dipole. The target, mounted on a thin substrate of aluminum or carbon, is 2 cm downstream from the window. Between these two a set of thin Al foils can be interposed to make small changes in beam energy. A pair of jaws can be moved radially in the middle of the dipole to define the horizontal acceptance of the particles emerging from the target. The whole chamber is insulated to act as a Faraday cup for the measurement of the beam current. The He gas enters at the target position to give additional cooling and is pumped away at the detector box. The constant renewal of the gas prevents the build-up of gaseous impurities which can affect the $\bar{q}$ of the evaporation residues.

Particle velocities can be measured by two transmission avalanche counters, located between the quadrupole doublet and the focal plane. For high Z and low velocities, multiple scattering in the windows and in the pentane gas of the counters increases the image size by a factor of two. This prohibits their use in experiments where a minimum image size is essential. The gas filling of

SASSY does not allow the use of counters which are based on the emission of secondary electrons.

The detector array in the focal plane consists of 5 surface barrier detectors to measure the energies of the implanted particles and their subsequent decays. A good position resolution is essential for time correlations of isotopes with long half-lives; therefore, the front contact of each detector is divided along the dispersion direction into 10 3-mm wide strips and the common rear contact is made resistive so that a position-sensitive signal can be obtained in the perpendicular direction. A position resolution of less than 1% thus gives in effect an array of 50 $\times$ 100 detector elements. Energy and position signals of the detectors are processed in a high energy branch for implantation of particles and fission decays and a low energy branch for alpha decays.

Any malfunction in the gas system triggers a fast closing valve that closes in 12 ms and holds a leak-tight seal between SASSY and the vacuum of the SuperHILAC.

For high beam intensity experiments a new electrostatic beam wobbler was installed 5 m upstream from SASSY. During a single beam pulse (5 ms) the beam spot moves on a ten turn spiral from the center of the target to the edge. The radius changes nonlinearly with time to give equal thermal stress over the whole target area.

4. Measurements of the Magnetic Rigidity

According to Ref. 8, the experimental average charge $\bar{q}$ of an ion passing through a dilute gas, can be parameterized by the following equation:

$$\frac{\bar{q}}{Z} = 1 - C_1 \exp\left\{-C_2\left(\frac{v}{v_o}\right)Z^{-2/3}\right\} . \tag{4}$$

The two parameters C_1 and C_2 are to be determined by a fit to experimental data. For $C_1 = C_2 = 1$ a first order expansion of the exponential gives the expression of Eq. 2. This relation of $\bar{q}$, Z and v is shown in Fig. 2 for all available data from Dubna,[5,12] Jülich[4] and LBL. Results from Ref. 4 have been used to normalize all data to He gas and to the same pressure. A fit to the data gives the values $C_1 = 1.04$ and $C_2 = 0.91$ for the parameters in Eq. 4. There are systematic deviations $\Delta\bar{q}/\bar{q}$ from the straight line of the order of $\pm 5\%$, which is about 3 times the experimental error.

For the superheavy element experiment, ^{48}Ca + ^{248}Cm, it was necessary to extrapolate Fig. 2 beyond the known range in order to make a reasonable prediction for an ion with Z = 116 and a velocity of $v/v_o = 2.22$. There is no obvious way to tell whether the systematic deviation of the data points in Fig. 2 results from a velocity or from a proton number (Z) dependence. So we selected two velocity ranges, $v/v_o = 4.0 \pm 0.5$ and $v/v_o = 2.2 \pm 0.5$ in order to investigate the Z dependence and the velocity dependence independently.

Figure 3 shows our experimental $B\rho/A$ values, which according to Eq. 1 for a constant velocity reflect mainly the dependence on $\bar{q}$. The atomic shell configurations as a function of the number of remaining electrons $N_e = Z - \bar{q}$ are shown for both velocity ranges. The configuration on top applies to the neutral atom.

The following conclusions can be drawn from Fig. 3:

(1)   The general trend of the Z dependence for both velocities is described by straight lines proportional to $Z^{-1/3}$. The slope $\dfrac{d\log\dfrac{B\rho}{A}}{d\log Z}$ is 0.48 for $v/v_o = 4$ and is 0.55 for $v/v_o = $

2.2. Imposed on this smooth trend are fluctuations which are closely related to the indicated shell structures.

(2) In the region of $Z = 72$ the relative maximum in $B\rho/A$ is shifted to higher Z for the higher velocity. But if we look at the maxima as a function of N_e rather than a function of Z, we note that the maximum seems to occur at the same number of remaining electrons. Maxima in $B\rho/A$ correspond to high ionization energy of the next electron to be removed and thus the systematic behavior is in close analogy to the isoelectronic sequences, known from atomic physics.

(3) Contrary to the prediction of Eq. 3 there is a velocity dependence of $B\rho$. The average difference of the $B\rho$ values is about 12%, but is much larger in the region of $Z = 70$ than in the region $Z = 82$.

(4) The influence of the atomic shells on the average charge $\bar{q}$ seems to decrease with increasing Z. This can be expected from the assumption that an infinite number of electrons can well be described by the Thomas-Fermi model.

(5) The shell effects seem to decrease for higher velocities. This is in accordance with results from energy loss experiments of α particles in different absorbers.[11]

(6) The extrapolation beyond $Z = 102$, which is shown for $v = 2.2\ v_o$ as a dotted line, is based on the similarities between the 4f-5d shell of the lanthanides and the 5f-6d shell of the actinides. The uncertainty in the magnetic rigidity at $Z = 116$ is about 10% corresponding to $\Delta B\rho/B\rho = \pm 5\%$, which is about one half of the width of the detector array of SASSY. This illustrates the required accuracy of our extrapolation.

Figure 3 also illustrates the previous difficulties in extrapolating the fission fragment data of the Z region between 36 and 60 toward higher Z. Petrov et al.[12] were the first to point out the strong deviation for $Z > 60$. Our data clearly substantiate their findings. The observed strong deviation of the average charge from a dependence $\bar{q} = \text{const} \times Z^{-1/3}$ also explains the difficulties

for Z identifications with energy loss measurements if $Z > 60$.[13] The different $B\rho/A$ values for the two velocity regions show that the velocity and the proton number (Z) have to be regarded as two independent parameters. Shell effects in the dependence of $\bar{q}$ as a function of velocity are discussed in Ref. 8. Our data, extending now beyond $Z = 100$, clearly demonstrate the importance of the atomic shell effects for $\bar{q}$ as function of Z.

5. Calculations of the Average Charge

To get more confidence in the empirical extrapolation to $Z = 116$, we tried to reproduce the fluctuations of $\bar{q}$ with an approach first proposed by Lamb.[10] He calculated the average charge of fission fragments by energetic considerations, rather than velocity considerations as Bohr[9] did. Lamb assumes that those atomic electrons are removed whose ionization potentials are lower than the kinetic energy transferred in the collisions between the gas atoms and the electrons of the ion. The kinetic energy transferred to the electrons in a central collision equals

$$E_k = (E/A)_i \cdot 4 \cdot m_e/m_n \; , \tag{5}$$

with $(E/A)_i$ the energy of the moving ion per nucleon and m_e/m_n the ratio of electron mass and nucleon mass.

This model does not consider the atomic structure of the gas or its density, but measurements from Jülich[4] and Dubna[5,12] show that both effects should result in a constant scaling factor. We cannot necessarily expect the absolute magnitude of $\bar{q}$ from the model, but with the ionization potentials as calculated by Carlson et al.[14] we find reasonable support of our findings and our phenomenological extrapolation. These ionization potentials are based on a shell model with the energy values and the radii taken from Hartree-Fock solutions of the neutral atom. A simple linear interpolation was used, giving

$$\bar{q} = q[I(n)] - \frac{I(n) - E_k}{I(n) - I(n+1)} \; , \tag{6}$$

with $I(n) > E_k > I(n+1)$ and $I(n)$ the ionization energy of the electron number n. This procedure means that the analytical velocity dependence of the Thomas-Fermi model is replaced by the energy dependence given by the set of tabulated ionization potentials. An average error of $\pm 5\%$ is quoted for the tabulated ionization potentials, with higher errors (up to 10%) for lower charge states. This error is propagated to an error in $\bar{q}$.

Equation 2 results in $\bar{q} \simeq \sqrt{I(n)}$ and hence $\Delta\bar{q}/\bar{q} \simeq 0.5 \, \Delta I(n)/I(n)$. We therefore expect an error for $\bar{q}$ which is of the same magnitude as the error for the calculated ionization energies.

It is not obvious whether a linear interpolation is appropriate, because quantum mechanically we expect a step function for $q(E_k)$. Especially at the transition of two main shells the steps are very unevenly spaced. But the velocity and the ionic charge distribution of the particles and the statistical nature of the interactions may justify a linear interpolation. The validity of the approach, first outlined by Betz,[8] was tested with data for Kr and Xe.

Figure 4 shows calculated and experimental average charges for Kr. The experimental average charges are predicted with good agreement. To test the model for a lower range in velocity, Fig. 5 shows measured and calculated values for the $B\rho$ dispersion as a function of energy of heavy mass fission fragments.[4] The calculation is made for Xe and it predicts with reasonable accuracy the increase of the velocity dispersion for energies corresponding to a velocity of $v/v_o < 3$.

Figure 6a shows the calculated $B\rho/A$ values for $v/v_o = 4$. We see a fairly good agreement between the experimental and the calculated Z-dependence. The shell structure is well reproduced in the Z range between 60 and 95. For smaller Z the calculation predicts some additional structures that are not observed in the experiment. The sharp kinks stem from the interpolation procedure.

For $v/v_o = 2.2$ the calculated charges are about one unit too small (Fig. 6b). This is in accordance with experimental results from Wittkover et al.[15] Except in the areas marked A and B the calculated values follow the oscillations of the experimental data. There is no quantitative way to remove the discrepancies at A or B but Wolke[16] has shown that for a series of light elements the removal of the first few electrons from a closed shell requires an excess of up to 100% over the estimated ionization energy. In our case an excess of about 20% would already completely remove the kinks at A and B.

6. Image Size

For a beam of particles, emerging from a thin target surface with an initial charge dispersion of $\Delta q/q$ and a velocity dispersion $\Delta v/v$, there are four independent contributions to the total image size in the focal plane:[3,4]

(1) Ion optical effects and target size,

(2) Velocity dispersion of the average charge $\bar{q}$,

(3) Charge exchange in the gas,

(4) Multiple scattering in the gas.

For the horizontal width of the image, all contributions are of roughly the same size for favorable operating conditions. The vertical width is independent of the velocity dispersion and the charge exchange. The ion optical contributions are determined by the magnification of the target size and by the aberrations caused by the ion optical elements. They were measured with an α-particle source at the target position with SASSY evacuated.

The velocity dispersion $\Delta B\rho/B\rho / \Delta v/v$ is a consequence of the deviation from proportionality of $\bar{q}$ and v (Eq. 2). An analytical expression for the velocity dispersion is obtained by differentiating Eq. 4. For pressures below 10 Torr, the energy loss is small and v can be assumed constant along the trajectory. Charge exchange and hence charge focusing increases with the pressure and its contribution[4] to the image size scales as given by Eq. 7.

$$\Delta B\rho/B\rho \text{ proportional to } \frac{\dfrac{\Delta q}{q}}{\sqrt{\Omega p}} , \tag{7}$$

where $\Delta q/q$ is the width of the charge distribution before the particles enter the gas. Ω is the effective charge exchange cross section and p the gas pressure. With an estimated $\Delta q/q$ of 24%, Ω was measured to be 16.3×10^{-18} cm^2 for $Z = 84$ and $v/v_o = 2.62$. From this value and experimental data from Refs. 6 and 8, the following dependence on v/v_o and Z was derived:

$$\Omega(Z,v)/cm^2 \ = \ 1.73 \ \left[\frac{v}{v_o}\right] - 1.12 \ Z^{0.75} \cdot 10^{-18} \ . \tag{8}$$

The effect of multiple scattering[17] is described by Eq. 9. Experimentally, it can be determined from the pressure dependence of the vertical image size.

$$\Delta B\rho/B\rho \ = \ 0.90 \ \left[\frac{v}{v_o}\right]^{-2} Z^{-0.23} \ p^{0.85} \quad \text{(p in mbar)} \ . \tag{9}$$

Adding quadratically all contributions to the image size the minimum of $\Delta B\rho/B\rho$ is determined by differentiation with respect to p. We obtain two useful scaling laws giving the dependence for $\Delta B\rho/B\rho$ and the optimum pressure, p_{opt} on the velocity v and the atomic number Z.

$$\frac{\Delta B\rho}{B\rho} \ = \ k_1 \ \left[\frac{v}{v_o}\right]^{-1} Z^{-0.21} \ , \tag{10}$$

$$p_{opt} \ = \ k_2 \ \left[\frac{v}{v_o}\right]^{1.15} \ , \tag{11}$$

The values of k_1 and k_2 depend on the design parameters of the separator system. The results of the calculations and their experimental verification are shown in Fig. 7a for Po recoils.

The reaction $^{162}Dy(^{40}Ar,2n)^{200}Po$ is a good test for the superheavy element reaction because low velocity recoils $(v/v_o = 2.6)$ are produced with reasonable cross section. The $\Delta B\rho$ width of the distribution of the EVR's in the focal plane of 40 mm and $p_{opt} = 0.5$ Torr are well predicted by Eqs. 10 and 11. The image size in the vertical direction is 16 mm. The calculation for the superheavy element reaction is shown in Fig. 7b. Note that the velocity dispersion now exceeds the contribution from ion optics. Equations 10 and 11 should not be extrapolated for velocities and atomic numbers which are higher than $v/v_o = 6$ and $Z < 40$.

Although the range of optimum pressure is relatively broad, we note that a minimum image size cannot be achieved for fusion reaction products and scattered particles simultaneously. The pressure is chosen to optimize the image size for the evaporation residues. For scattered atoms the optimum pressure would be higher but the optimum width is smaller, so we may expect about the same width for both distributions. If the distributions are Gaussian in both directions, the

efficiency of collecting an evaporation residue is about 45% for a detector the dimensions of which are comparable with the horizontal and vertical half-width of the spatial distribution of the particles.

7. Separation Characteristics

Knowing the magnetic rigidity and the image size as a function of energy we can estimate the separation between evaporation residues, scattered target atoms and beam particles for a particular reaction. We assume that in the worst case projectiles and scattered target atoms with energies from the maximum value down to zero are scattered into the EVR path. It follows from Fig. 5 for the case of Xe, that there is always an increase in $B\rho$ for low energies with the actual values depending on the specific nucleus. Figure 8 shows the situation for the superheavy element reaction ^{48}Ca + ^{248}Cm. In this case the $B\rho$ value for the evaporation residues is taken from Fig. 3 and the implantation energy is 36 MeV from reaction kinematics. This defines the hatched area in Fig. 8.

The $B\rho$ values for the Ca beam were calculated with Eq. 4. The two data points for Cm were taken from experiments with elastically scattered Cm. The position sensitive detector allowed the determination of the energy dependence of $B\rho$. For a Cm energy of 34 MeV we found a variation of 2% in $B\rho$ for an energy variation of 33%. This finding is in good agreement with a calculation similar to the Xe case in Fig. 5. The graphs for Ca and Cm in Fig. 8 show the expected ridges of the intensity distributions. The actual background in the detectors is determined by the width of the distributions in vicinity of the hatched area. In the energy window of the EVR's the separation of the Cm recoils from the EVR's in the $B\rho$-focal plane is about twice the calculated image size.

An evaluation of earlier SASSY experiments with heavy targets gives an average rate of background events in the energy region of expected evaporation residues of about 0.2 counts/sec at 1 μA beam current, almost independent of the target-projectile combination. This has the consequence that evaporation residues with cross sections smaller than 1 μbarn can be detected only by a link to subsequent decay chains, a technique first described by Schmidt et al.[18] and applied later to the detection of elements 107−109.

8. Experimental Results for the Reaction ^{48}Ca + ^{208}Pb

The high cross section for the reaction ^{48}Ca + ^{208}Pb $\rightarrow$ ^{254}No + 2n made it a suitable reaction to obtain a charge calibration point for Z = 102 and to investigate the separation capabilities of SASSY. A comparison with the previously measured cross section allows a rough determination of the transmission through SASSY. The target consisted of 400 μg/cm^2 enriched ^{208}Pb and the average ^{48}Ca beam was about 30 particle nanoamperes. The energy loss for a 250 μg/cm^2 Al beam window and a 250 μg/cm^2 Al target backing was calculated with the Hubert tables.[19]

The energy spectrum in Fig. 9 shows the sum of all events in the detector array for a single beam energy close to the maximum of the excitation function. The three peaks of full energy projectiles, scattered target particles and evaporation residues are clearly separated. From the intensities the separation characteristics were deduced. The transmission for full energy Ca projectiles is 10^{-15}. A comparison with gas-jet data[20] shows that the transmission for target-like alpha emitters is $<10^{-3}$. Even for the highest bombarding energies above 230 MeV, there was no alpha line at 11.6 MeV, which would indicate the detection of ^{212m}Po. The distribution of events along the focal plane is shown in Fig. 10. As discussed in Section 6, most of the events associated with projectiles and target are to be found in the detectors located at smaller Bρ values. Figure 11 shows the alpha spectrum. Only alpha-events outside of the macropulse of the SuperHILAC were recorded. ^{254}No and its daughters ^{250}Fm and ^{246}Cf were observed. Label "Tra" denotes long-lived transfer products in the At region.

The experimental excitation function (Fig. 12) can be compared to earlier investigations of the ^{48}Ca + ^{208}Pb reaction in Dubna[21] and Berkeley.[20] A re-evaluation of the energy loss in the gas-jet experiment[20] gives good agreement with our result of 211 $\pm$ 2 MeV for the maximum of the excitation function. This value and the width of 9 MeV are in approximate agreement with HIVAP-calculations by Hessberger[22] predicting 218 MeV and a width of 8 MeV. These calculations also explain why the 2n channel is by far the most abundant channel in the reaction. A

comparison with the experimental cross sections (Table 1) from Refs. 20 and 21 allows one to determine an approximate transmission of evaporation residues through SASSY.

The total efficiency, W_{TOT}, for the detection of full energy alpha particles emitted by implanted EVR's can be expressed as the product of three efficiencies,

$$W_{TOT} = W_{TRANS} \times W_{DET} \times W_\alpha .$$

W_{TRANS} is the efficiency for an EVR to reach the focal plane after passing through collimators, grids, etc. Since the principal objective of this experiment was to determine accurately the magnetic rigidity for $Z = 102$, a central collimator was used in the bending magnet. This restricted the horizontal acceptance to $\pm 1\,^\circ$ and as a result W_{TRANS} must be regarded as uncertain.

W_{DET} is the efficiency of the detector in covering the focal plane area where the EVR's are focussed. It depends on the size and number of Si detectors and their supports. For this experiment we used ten crystals, each 5 mm wide and 20 mm high and each surrounded by a 1 mm border. No attempt was made to determine the size of the focal plane image because of the small amount of activity available in this experiment.

W_α is the efficiency of the detector in producing a full energy alpha signal after implantation of an EVR. Since the EVR is usually implanted to a depth of the order of 2 mg/cm^2 Si the geometry for stopping an alpha particle emitted by the EVR will be somewhat greater than 2π. Typical values will vary from 53% for an 11-MeV alpha to 58% for an 8-MeV alpha. We will assume 58% for the 8.1-MeV alphas of ^{254}No. Included in W_α are any duty cycle limitations. In this particular case counting was done only in the intervals between beam pulses--an 85% duty cycle.

Thus W_α for this experiment was 0.58 $\times$ 0.85 = 0.49 or 49%.

To determine W_{TOT} we compared the yield of ^{254}No in this experiment with that found at LBL in 1976 for the same reaction but using a helium gas-jet system for analysis.[20] In that

experiment the cross section was measured to be 3.4 ± 0.4 μb, assuming that the gas-jet yield was 60%. This should be compared with the value 3.8 ± 0.8 μb measured earlier at Dubna.[21] In the SASSY experiment we observed 0.13 ± 0.01 alpha counts of ^{254}No per μC of ^{48}Ca^{14+} at the peak of the excitation function. A 3.4 μb cross section would produce 1.7 atoms per μC. Thus W_{TOT} is $\frac{0.13}{1.7} = 0.076$ or 7.6% for the overall efficiency in terms of alpha counts detected per number of atoms formed. Since W_{α} must be close to 49% we can deduce that

$$W_{TRANS} \times W_{DET} = \frac{0.076}{0.49} = 0.155 \quad \text{or} \quad 15.5\% \ .$$

Assuming a reasonable value for W_{DET} of 50% from other experiments we obtain the value $\frac{0.155}{0.50} = 0.31$ or 31% for W_{TRANS}. Considering the various uncertainties in this experiment which was not designed specifically to determine yield, this value is in reasonable accord with that to be expected from the calculations.

9. Experimental Results for the Reaction ^{48}Ca + ^{248}Cm

In a recent collaboration between LBL (Lawrence Berkeley Laboratory, Berkeley) and GSI (Gesellschaft für Schwerionenforschung, Darmstadt), and others, the possible production of superheavy elements with Z = 116 in the reaction ^{48}Ca + ^{248}Cm was studied.[23] Various chemical methods were used, as well as the two on-line separators, SASSY and SHIP.[1]

As far as detection of superheavy nuclei is concerned, the result of the experiment was negative. However, the gas-filled separator was shown to be capable of fairly background-free operation, and an upper limit for the production cross section of roughly 3×10^{-34} cm^2 was obtained for a half-life range of a few microseconds to several seconds.

In addition, the applicability of the correlation technique was demonstrated by the observation of alpha decay chains starting from isotopes slightly heavier than ^{208}Pb, most notably ^{222}Ra, ^{219}Rn, and ^{220}Rn. The study of the multinucleon transfer mechanism responsible for the production of these isotopes would be of interest, in particular because the other partner in such fragmentation processes might be a neutron-rich isotope of mass close to 70, such as ^{73}Zn or ^{70}Ni.[24]

10. Conclusions

The experimental data for the efficiency for the detection of evaporation residues and for the suppression of background show that SASSY compares well with other separation methods. Table 1 shows a comparison of several significant parameters for SASSY and the velocity filter SHIP,[1,25] whose outstanding performance is well known.[26] When on-line separators are used for the detection of new activities, the identification is ideally based on the observation of time- and position-correlated alpha decay chains with previously known radioactive isotopes. This technique[18] which has proved efficient and dependable in particular in the search for new elements using SHIP,[26] is also well suited for work using a gas-filled separator. When the suppression of interfering heavy particles is sufficient, the performance of the system is mainly determined by the position and energy resolution of the focal plane semiconductor detector.

11. Acknowledgement

12. References

1. G. Münzenberg, W. Faust, S. Hofmann, P. Armbruster, K. Güttner, H. Ewald, Nucl. Instr. Meth. *161* (1979) 65.

2. B.L. Cohen, C.B. Fulmer, Nucl. Phys. *6* (1958) 547.

3. P. Armbruster, Nucleonika *3* (1961) 188.

4. H. Lawn, J. Eidens, J.W. Borgs, R. Fabbri, J.W. Grüther, G. Joswig, T.A. Khan, W.D. Lauppe, G. Sadler, H.A. Selic, M. Shaanan, K. Sistemich, P. Armbruster, Nucl. Instr. Meth. *137* (1976) 103.

5. V.A. Karnaukhov, L. Rubinskaya, G. TerAkop'Yan, V. Titov, V.A. Chugreev, JINR P13-4454, Dubna 1969; I. Bacho, D.D. Bogdanov, Sh. Dorotsi, V.A. Karnaukhov, L.A. Petrov, G.M. TerAkop'Yan, JINR P13-4453, Dubna 1969.

6. P. Armbruster, J. Eidens, J.W. Grüther, H. Lawin, E. Roeckl, K. Sistemich, Nucl. Instr. Meth. *91* (1971) 499.

7. M.E. Leino, S. Yashita, A. Ghiorso, Phys. Rev. C*24* (1981) 2370; M. Leino, Dissertation, Report Series in Physics HU-P-D37, University of Helsinki, 1983, S. Yashita, thesis, LBL-15562 (1984).

8. H.D. Betz, Rev. Mod. Phys. *44* (1972) 465.

9. N. Bohr, Phys. Rev. *59* (1941) 270.

10. W.E. Lamb, Phys. Rev. *58* (1940) 696.

11. J.F. Ziegler, Helium Stopping Powers and Ranges of all Elements in Matter, Pergamon Press 1977.

12. L.A. Petrov, V.A. Karnaukhov, D.D. Bogdanov, Sov. Phys. JETP *32* (1971) 1042.

13. P. Glaessel, R.C. Jared, L.C. Moretto, LBL-5064, Berkeley 1976.

14. T.A. Carlson, C.W. Nestor, N. Wassermann, F.D. McDowell, Atomic Data *2* (1970) 63 and T.A. Carlson, C.W. Nestor, F.D. McDowell, ORNL-4721 (Oak Ridge 1971).

15. A.B. Wittkower, H.D. Betz, Phys. Rev. A *7* (1973) 159.

16. R.L. Wolke, Phys. Rev. *171* (1968) 301.

17. P. Belery, T. Delbar, G. Gregoire, Nucl. Instr. Meth. *179* (1981)

18. K.-H. Schmidt, W. Faust, G. Münzenberg, H.-G. Clerc, W. Lang, K. Pielenz, D. Vermeulen, H. Wohlfarth, H. Ewald, K. Güttner, Nucl. Phys. *A318* (1979) 253.

19. F. Hubert, A. Fleury, R. Bimbot, D. Gardes, Ann. Phys., Fr. Vol. 5, Supplement (1980) 3.

20. J.-M. Nitschke, R.E. Leber, M.F. Nurmia, A. Ghiorso, Nucl. Phys. *A313* (1979) 236.

21. O.A. Orlova, H. Bruchertseifer, Y.A. Muzychka, Y.T. Oganessian, B.I. Pustylnik, C.M. TerAkop'Yan, Sov. Nucl. Phys. *30* (1979) 317. A. Türler, H. Gäggeler, K. Sümmerer, GSI - Nachrichten 07-86 (1986) 7.

22. F.P. Hessberger, GSI-Report, GSI-85-11, 1985.

23. P. Armbruster, Y.K. Agarwal, W. Brüchle, M. Brügger, J.-P. Dufour, H. Gäggeler, F.P. Hessberger, S. Hofmann, P. Lemmertz, G. Münzenberg, K. Poppensieker, W. Reisdorf, M. Schädel, K.-H. Schmidt, J.H.R. Schneider, W.F.W. Schneider, K. Sümmerer, D. Vermeulen, G. Wirth, A. Ghiorso, K.E. Gregorich, D. Lee, M. Leino, K.J. Moody, G.T. Seaborg, R.B. Welch, P. Wilmarth, S. Yashita, C. Frink, N. Greulich, G. Herrmann, U. Hickmann, N. Hildebrand, J.V. Kratz, N. Trautmann, M.M. Fowler, D.C. Hoffman, W.R. Daniels, H.R. von Gunten, H. Dornhöfer, Phys. Rev. Lett. *54* (1985), 406.

24. P. Armbruster, Y.K. Agarwal, A. Ghiorso, S. Hofmann, F.P. Hessberger, M. Leino, K. Moody, G. Münzenberg, K. Poppensieker, W. Reisdorf, K.-H. Schmidt, J.H.R. Schneider, W.F.W. Schneider, D. Vermeulen, GSI Scientific Report 1983, p. 81.

25. G. Münzenberg, W. Faust, F.P. Hessberger, S. Hofmann, W. Reisdorf, K.-H. Schmidt, W.F.W. Schneider, H. Schott, P. Armbruster, K. Guttner, B. Thuma, H. Ewald, D.

Vermeulen, Nucl. Instr. Meth. *186* (1981) 423.

26. G. Münzenberg, P. Armbruster, F.P. Hessberger, S. Hofmann, K. Poppensieker, W. Reis-
dorf, J.H.R. Schneider, W.F.W. Schneider, K.-H. Schmidt, C.C. Sahm, D. Vermeulen, Z.
Phys. *A309* (1982) 89.

Table 1. Comparison of the velocity filter SHIP and the gas-filled separator SASSY for fusion reactions. The data for both devices are reaction dependent.

	SHIP	SASSY
Acceptance		
relative ionic charge	20%	100%
relative recoil velocity	10%	40%
Area for 50% detection of the distribution for evaporation residues in the focal plane	40×20 mm	50×20 mm
Suppression of full energy beam particles	$10^{12} - 10^{17}$	$\sim 10^{15}$*
Suppression of quasielastic transfer products and target knock-outs	10^4	$> 10^3$
Experimental efficiency for full energy α detection; highly dependent on detector size	10—20%	15—60%

*Depending on reaction and beam.

Figure Captions

Fig. 1. Schematic representation of SASSY. The evaporation residues move in the hatched area. Target and beam trajectories are shown for heavy target recoils and light beam.

Fig. 2. Parameterization for the average charge $\bar{q}/Z$ according to Eq. 4. The velocity range is $1.5 < v/v_0 < 4.5$ and the Z range is $36 \leq Z \leq 102$. Slow (1.5 .. 3.0) and fast (3.0 .. 4.5) denote the lower and upper half, respectively, of the velocity interval.

Fig. 3. Experimental values for $B\rho/A$ as a function of Z the atomic number of the ions. The smooth line through the data points is only to guide the eye, the straight lines are fits to the data points to show the trend $\sim Z^{-1/3}$. The electron configurations of the ions are shown, the configuration on the top frame applies to the neutral atom. Uncertainties in the experimental values are of the size of the data points. The point in parenthesis at $Z = 92$ and $v/v_0 = 3.33$ is slightly outside the velocity interval.

Fig. 4. Experimental data for the average charge of ^{36}Kr in comparison to the theory of Bohr (Eq. 2) and the calculation with the Ionization Potential (Eq. 6).

Fig. 5. Dispersion of $B\rho$ as a function of energy for heavy fission fragments,[4] compared to the calculation with ionization potentials (Eq. 6). The calculation was made for ^{140}Xe. The error bars for the experimental points are estimated from the line width, the errors for the calculated values are based on the quoted average error of 5% for the Carlson tables.[13] There is no normalization in the two curves.

Fig. 6. a) Calculated values for $B\rho/A$ with Eq. 6, compared to the experimental data for v/v_0 = 4.0. b) Same as (a) for $v/v_0 = 2.2$. Experimental data points as in Fig. 3. The insert in Fig. 6(b) shows the differences between experimental and calculated average charges for all calculations performed.

Fig. 7.   a) Calculated and experimental width for the evaporation residues with Z = 84 and

v/v_o = 2.6 from the reaction ^{40}Ar + ^{164}Dy. The arrows denote the minimum values for

the width. b) Calculated width of the distribution at the focal plane for the evapora-

tion residues Z = 116 and v/v_o = 2.2 from the reaction ^{48}Ca + ^{248}Cm.

Fig. 8. $B\rho$ values as a function of kinetic energy for the reaction ^{48}Ca + ^{248}Cm. The ($B\rho$-E)

window for evaporation residues is the hatched area. The $B\rho$ value for Ca is based on

the extrapolation shown in Fig. 3 and Eq. 4.

Fig. 9.   Energy spectrum of implanted particles, obtained with the focal plane detector in the

reaction ^{48}Ca + ^{208}Pb. No time coincidence windows.

Fig. 10.   Intensity distribution in the focal plane of evaporation residues, alpha particles, elasti-

cally scattered target atoms and full energy beam particles for the reaction

^{48}Ca + ^{208}Pb. $B\rho$ increases to the left and each detector is approximately 5 mm wide,

equivalent to 1% in $B\rho$.

Fig. 11.   Alpha decays in the focal plane detector for the reaction ^{48}Ca + ^{208}Pb. Only counts

outside the beam pulse time window are taken, but without correlation. TRA denotes

transfer products in the At-region. The fit is a calculation with the known half-life of

55 s.

Fig. 12.   Excitation function for the 2n reaction, ^{48}Ca + ^{208}Pb $\rightarrow$ ^{254}No. The error bars for the

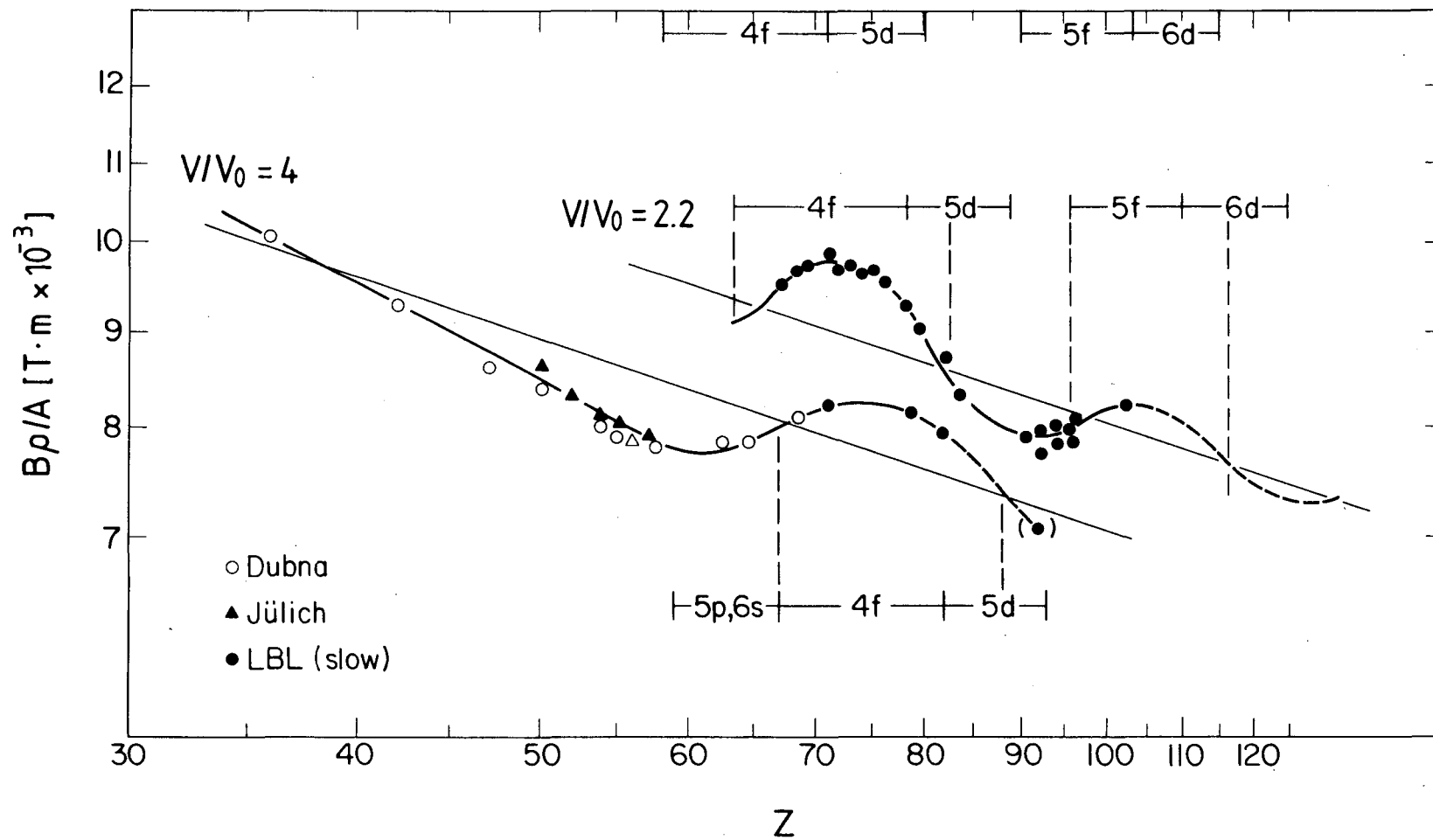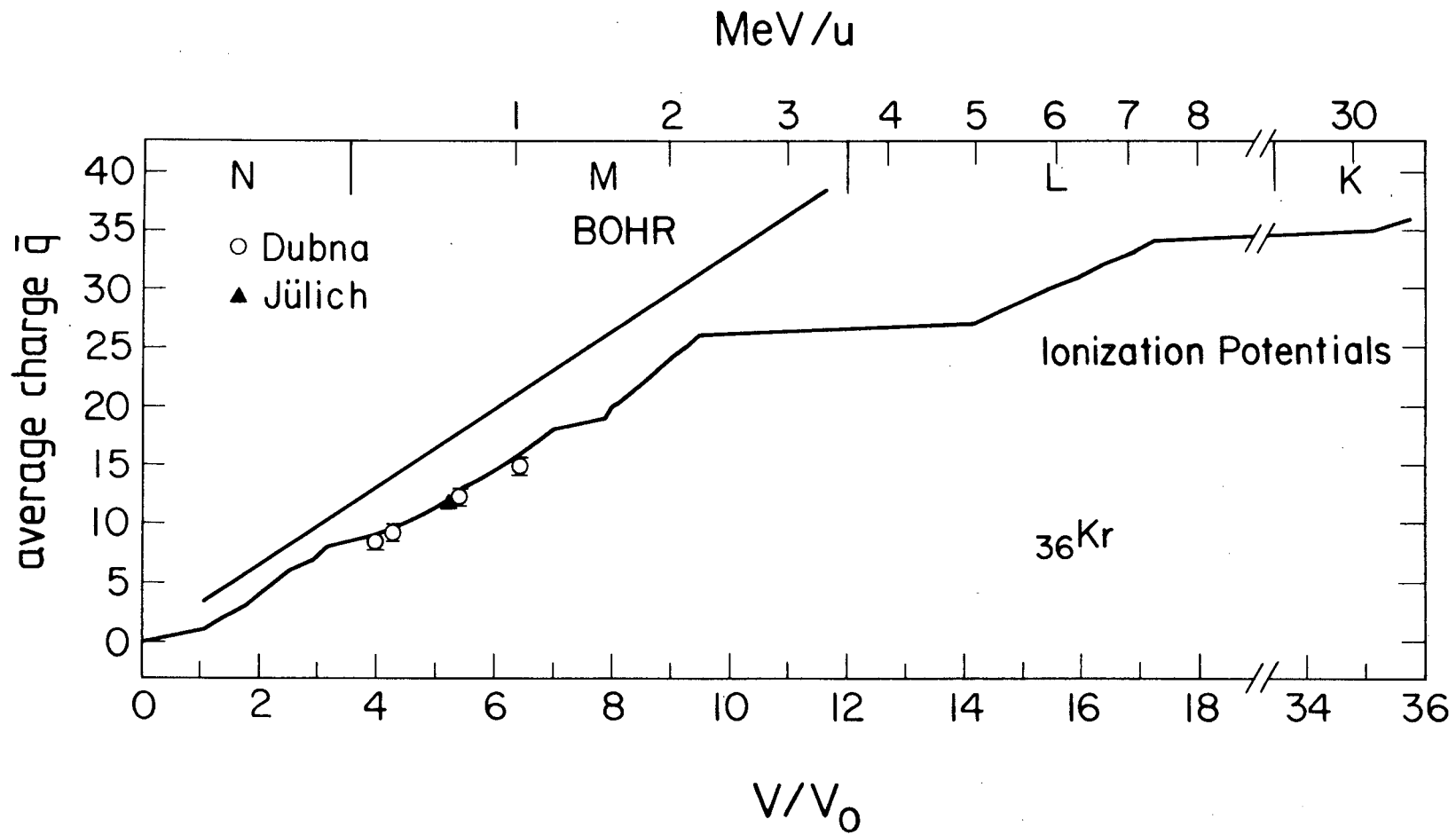energy reflect the uncertainty in the absolute energy determination.

XBL 837-2814

Fig. 1

$$(1-\bar{q}/Z)=1.04 \exp-(0.91 Y_0)$$

Legend (on figure):
- ○ Dubna
- ▲ Jülich
- ● LBL (slow)
- ▽ LBL (fast)

Y-axis: Logarithm $\ln(1-\bar{q}/Z)$
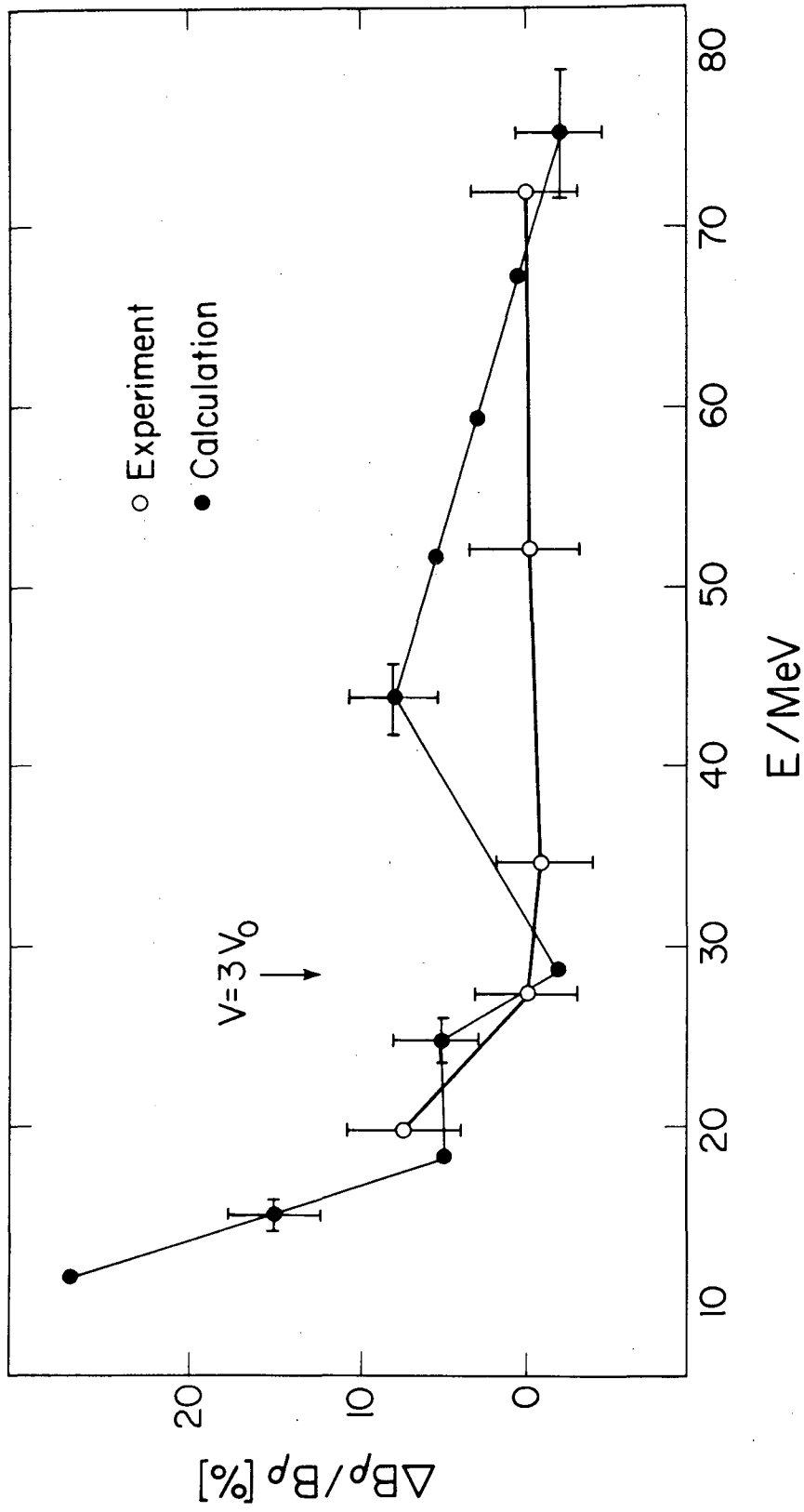
X-axis: $Y_0 = (V/V_0) \cdot Z^{-2/3}$
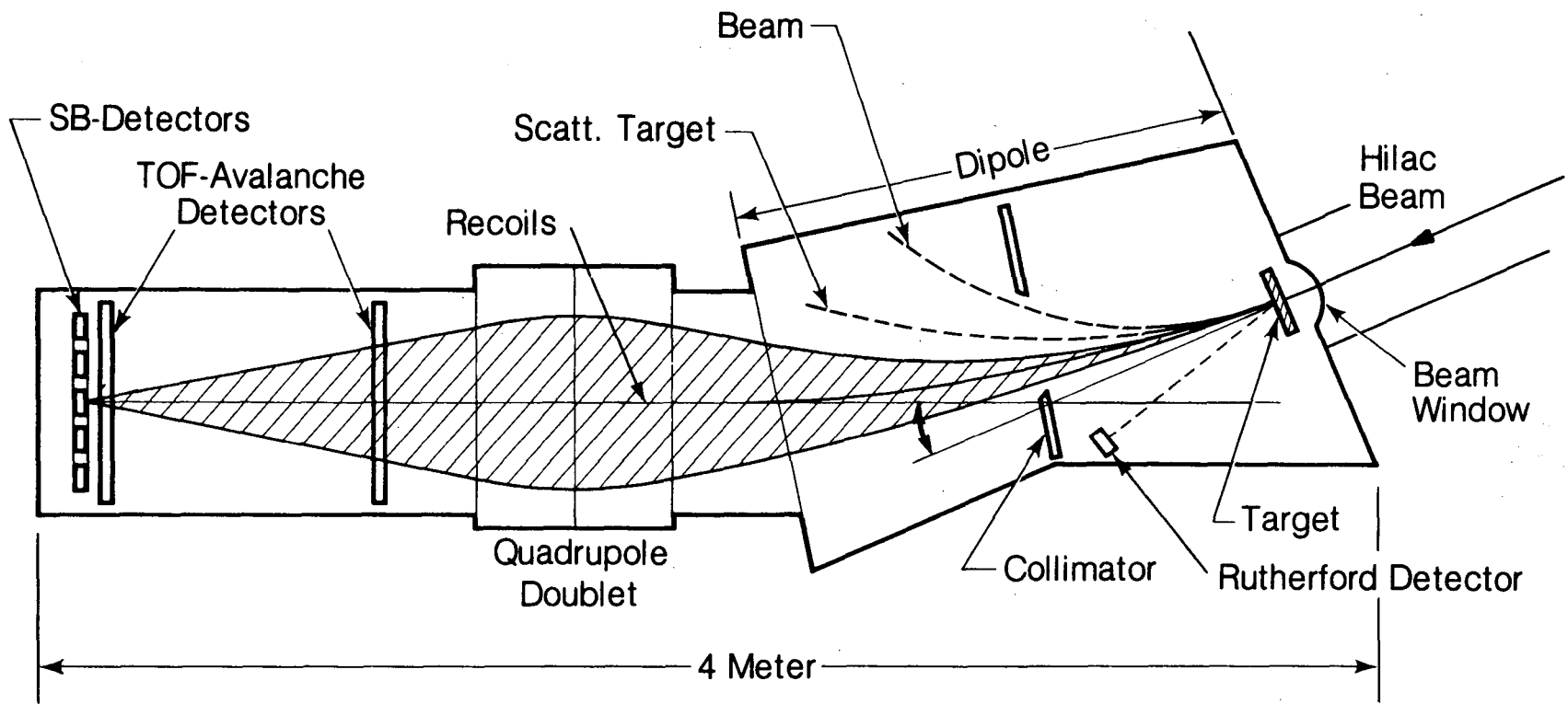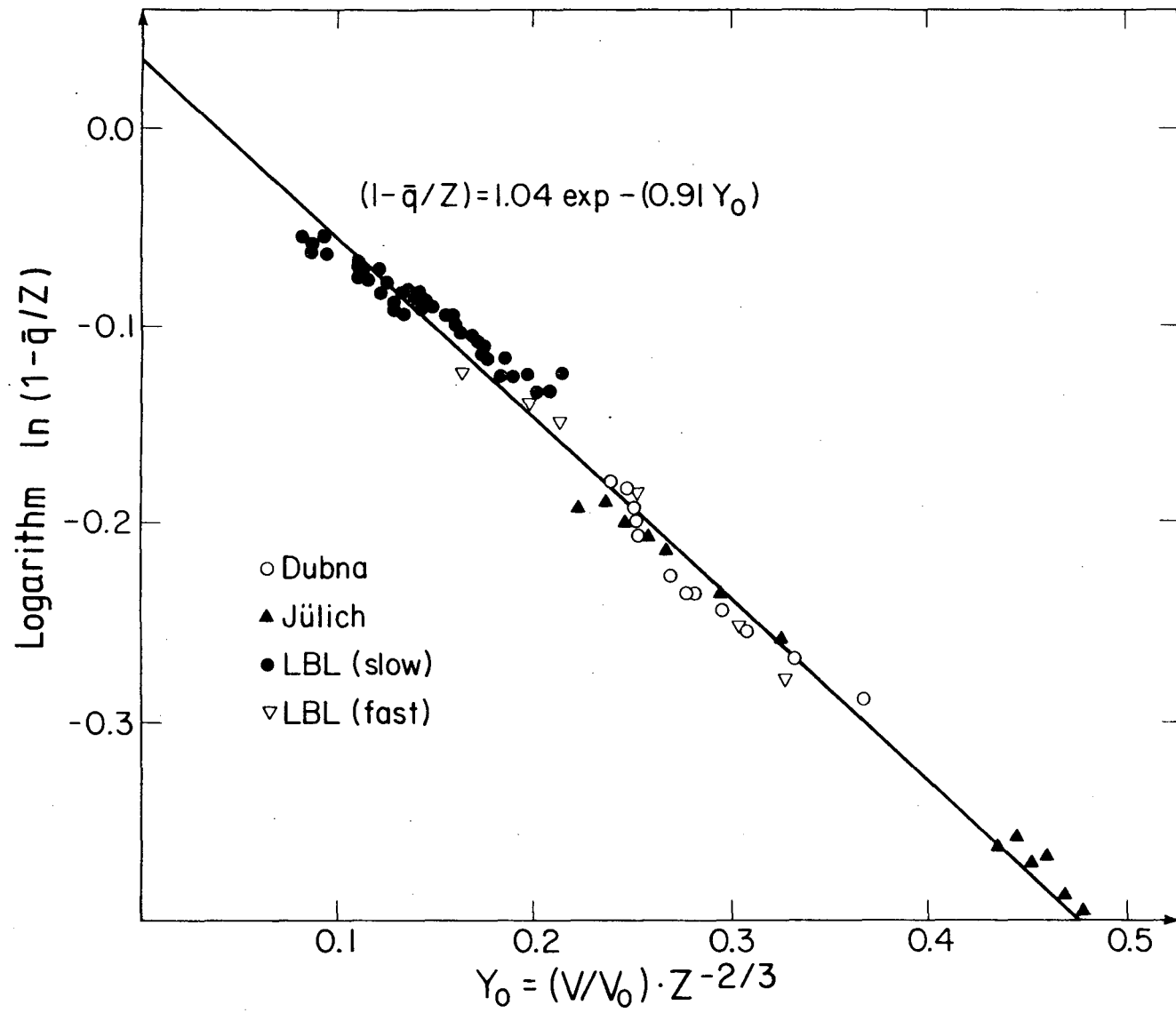
XBL 834-1553
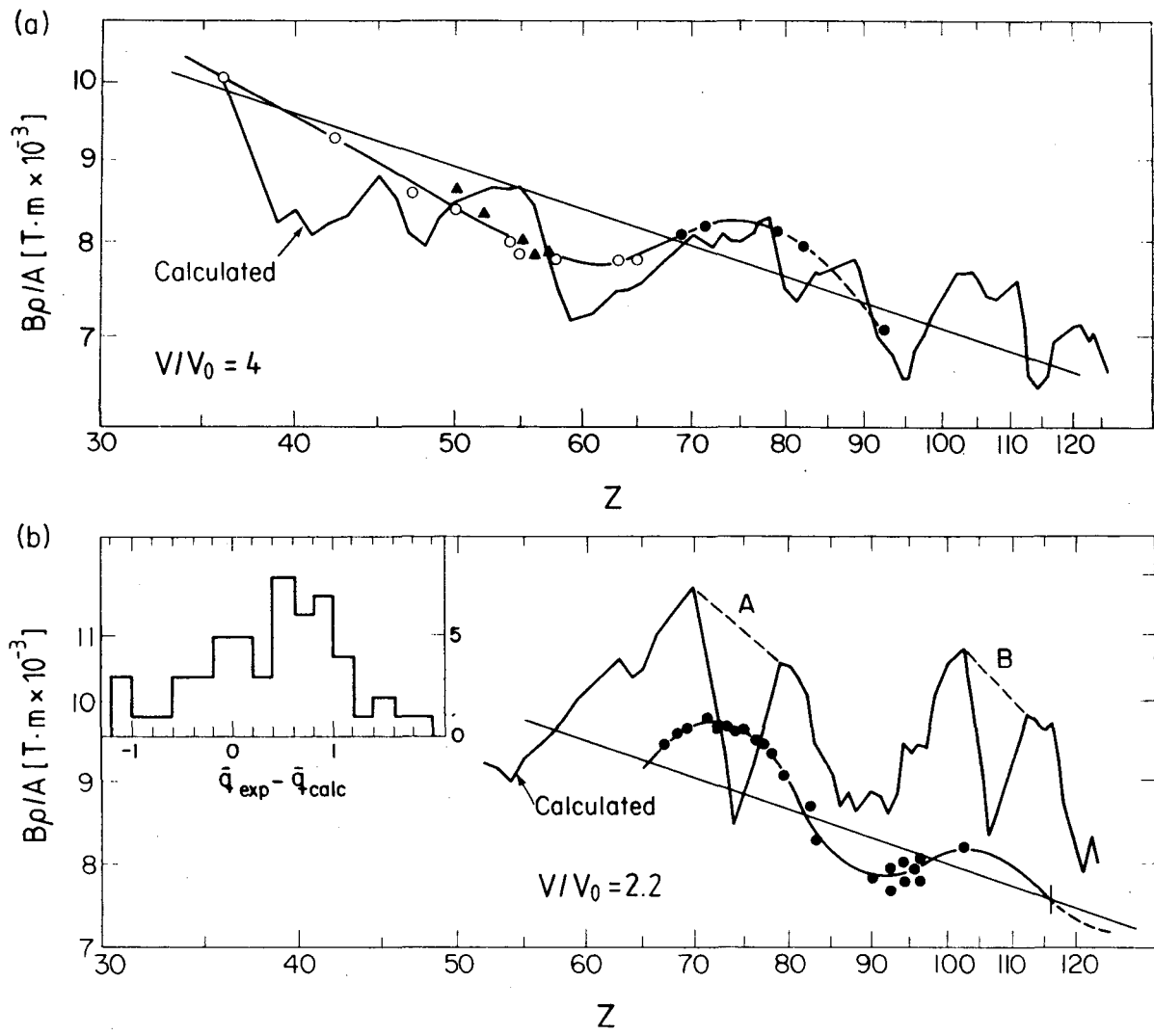
Fig. 2

Fig. 3

XBL 834-1552

Fig. 4

Fig. 5
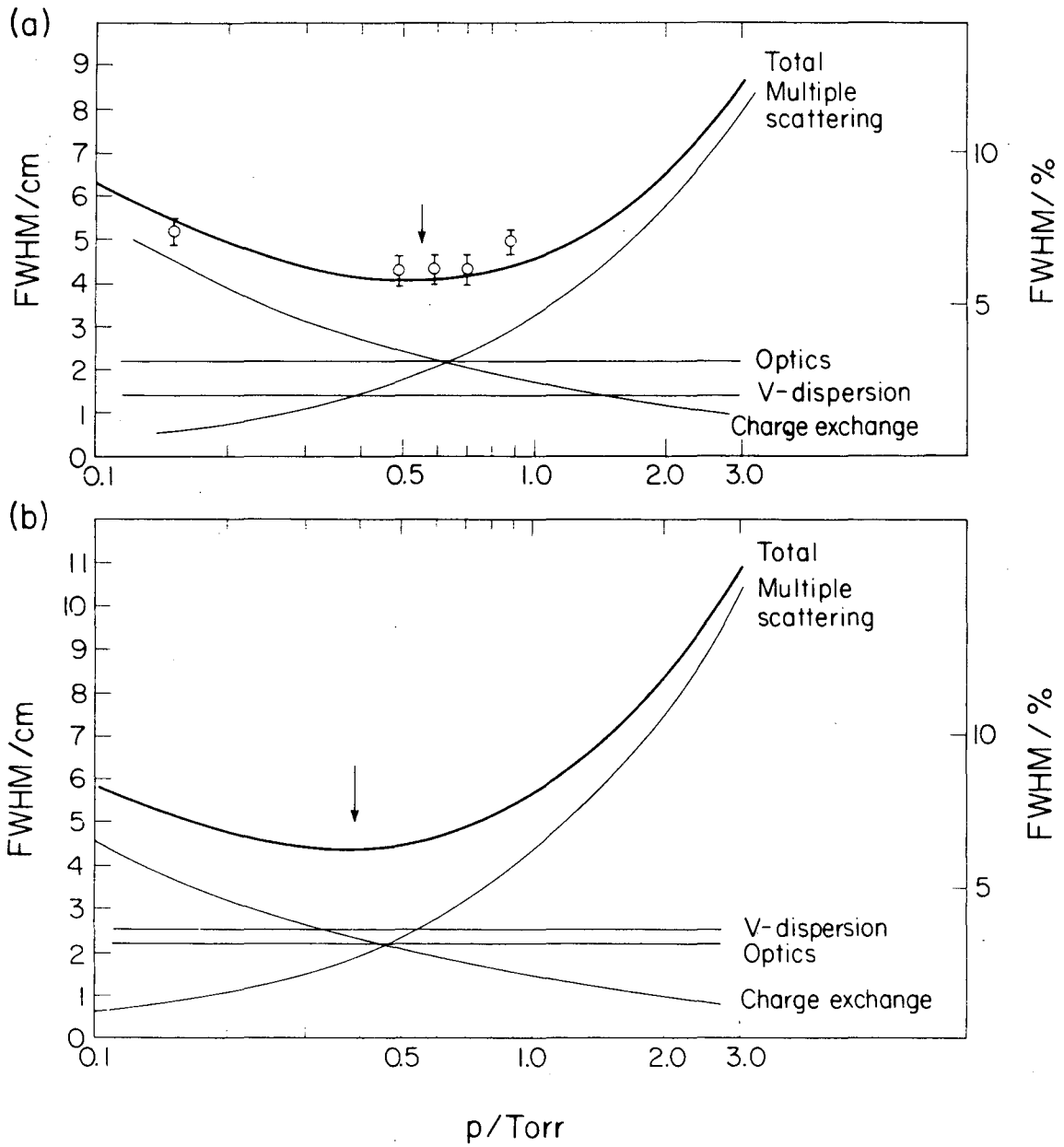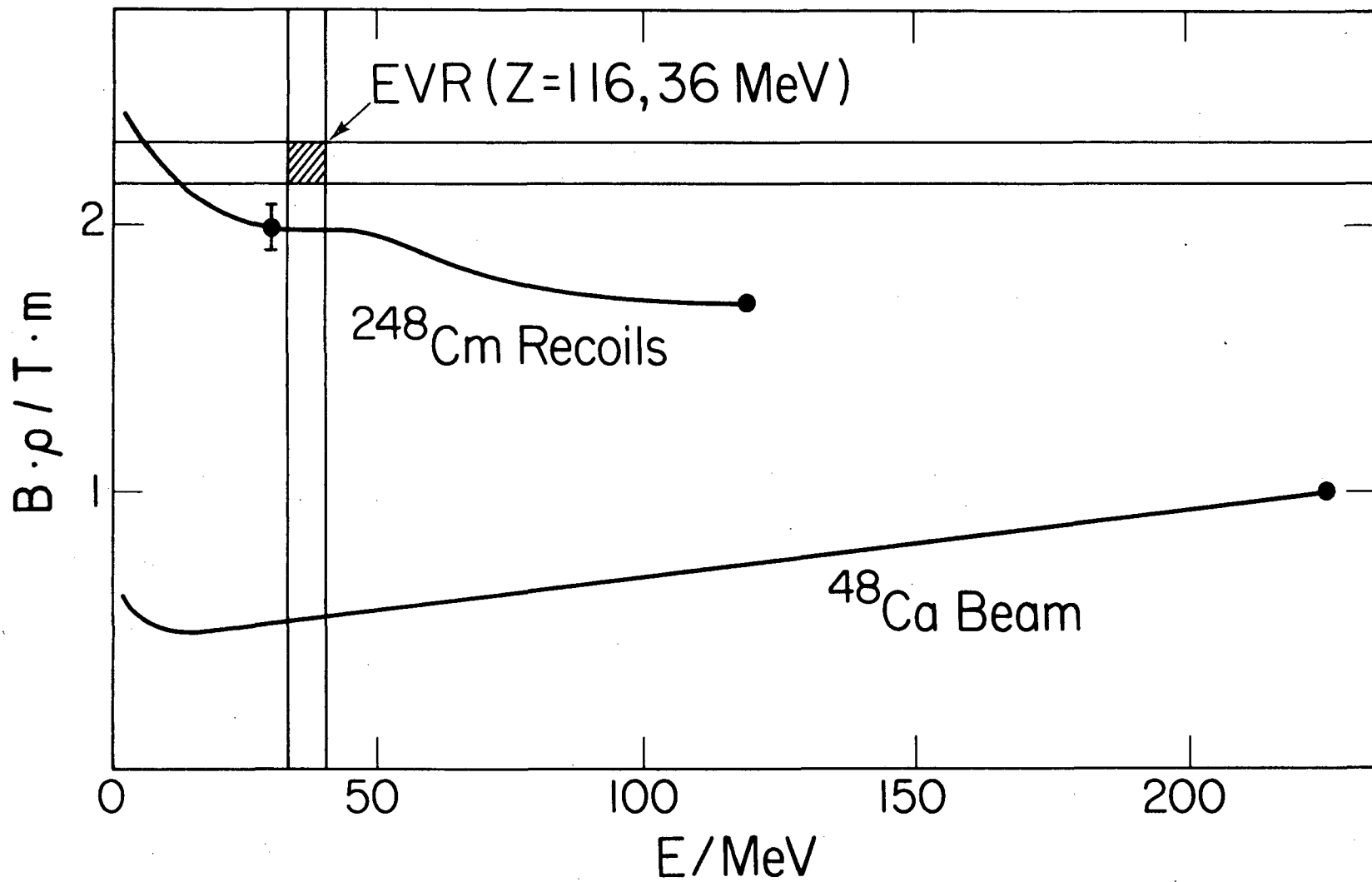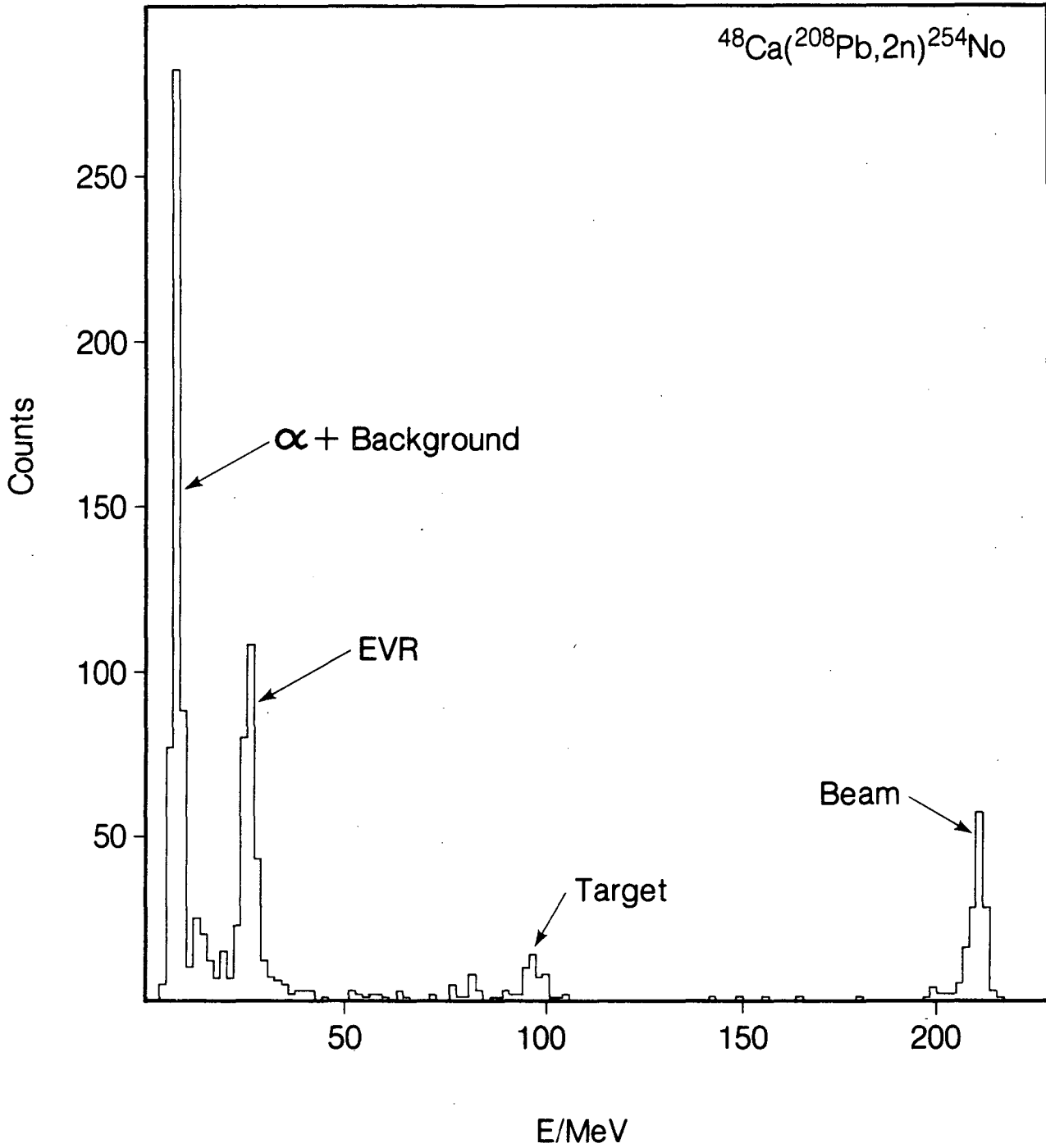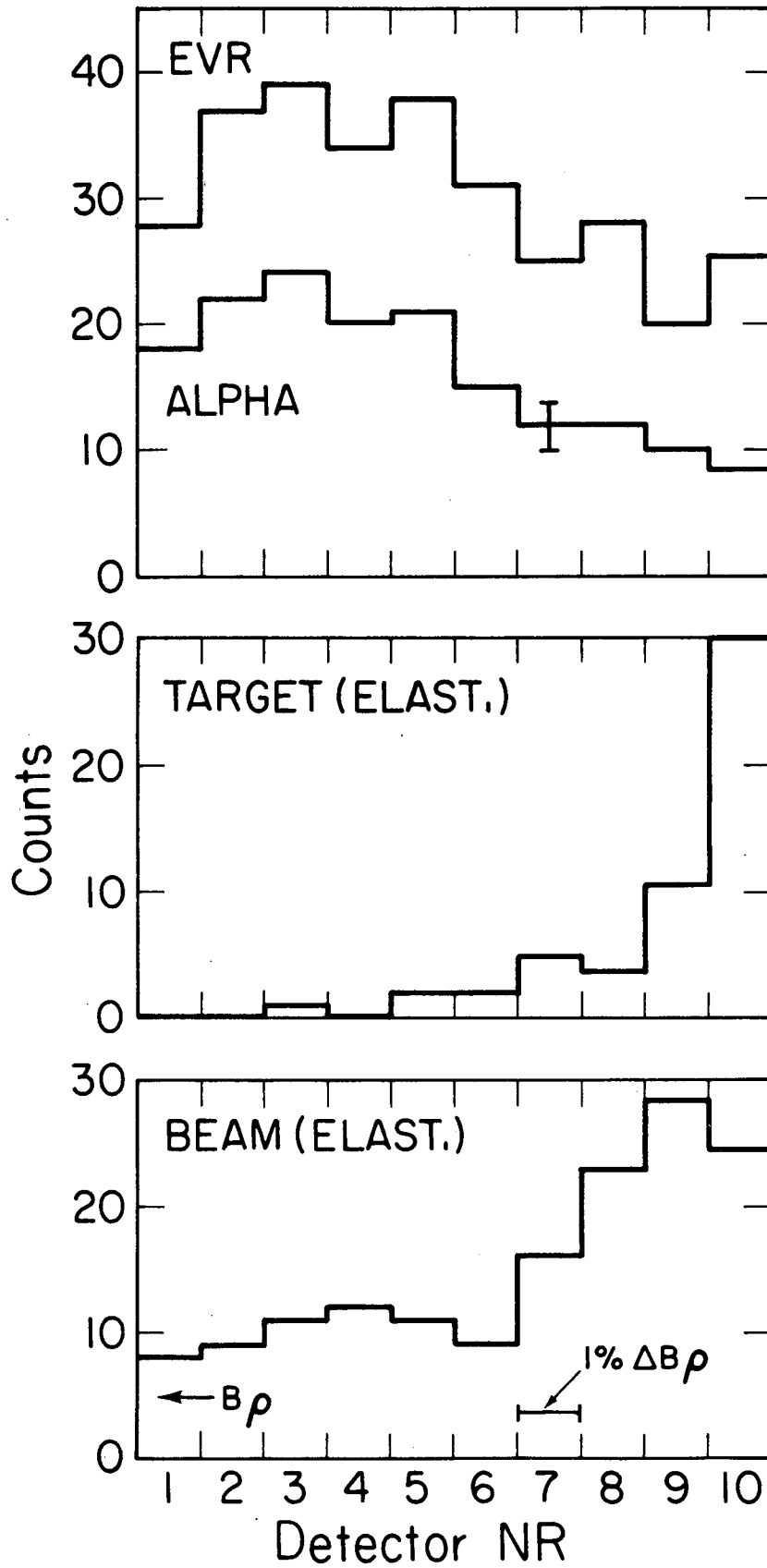
XBL 834-1549

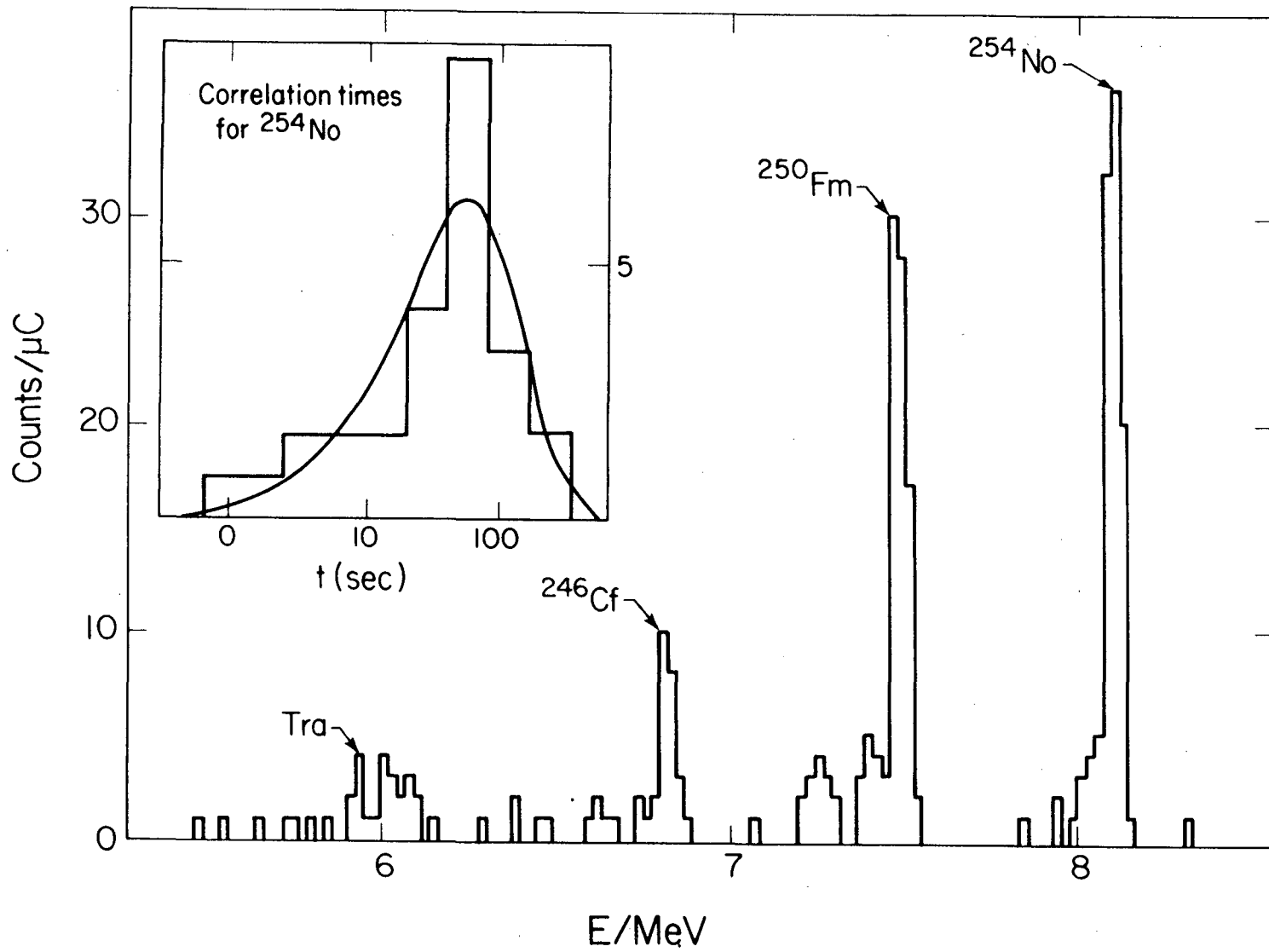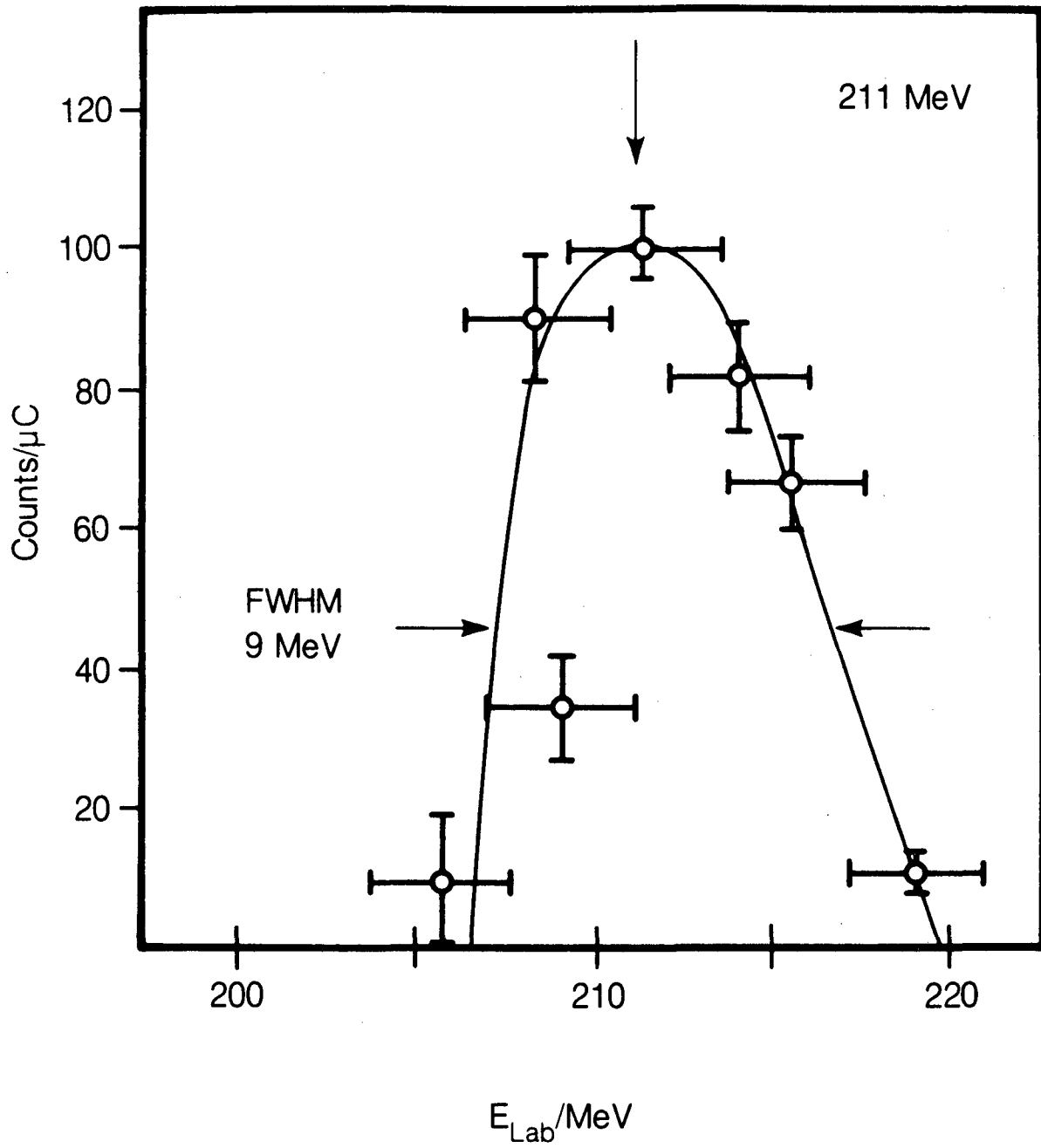Fig. 6

XBL 834-1550 A

XBL 834-1613

Fig. 7

Fig. 8

Fig. 9

XBL 837-1893

Fig. 10

Fig. 11

-38-

XBL 8710-4168

Fig. 12